

CFD STUDY ON SPECIAL DUTY CENTRIFUGAL PUMPS OPERATING WITH VISCOUS AND NON-NEWTONIAN FLUIDS

C. Buratto^a - M. Pinelli^b - P.R. Spina^c - A. Vaccari^d - C. Verga^e

Engineering Department in Ferrara (EnDiF), Ferrara, Italy

^acarlo.buratto@unife.it, ^bmichele.pinelli@unife.it, ^cpier.ruggero.spina@unife.it,
^danna.vaccari@unife.it, ^eclaudio.verga@unife.it

ABSTRACT

Centrifugal pump design operating with special fluids (high viscosity, non-Newtonian, solid handling) is usually performed by considering water as the working fluid and then by applying empirical correction to the performance according to the fluid processed. CFD techniques allow the analysis of the impact of the fluid properties and the effectiveness of the design correction, rather than only relying on specific empirical data for each specific fluid.

In this paper, a CFD analysis is performed on a large-size industrial food processing centrifugal pump originally designed for tomato paste. A model sensitivity analysis on the fluid constitutive law and on the flow regime modeling (laminar or turbulent) was performed. The CFD study showed that a fluid viscosity increase affects pump performances coherently with literature data. Then, pump curves and 3D flow structures obtained with non-Newtonian fluid are similar to those obtained with high viscous Newtonian fluids.

NOMENCLATURE

$\dot{\gamma}$	shear deformation rate, $\partial u/\partial y$	BEP	Best Efficiency Point
$\dot{\gamma}_{max}$	upper boundedness deformation limit for Ostwald De Waele model	g	gravity acceleration
$\dot{\gamma}_0$	lower boundedness deformation limit for Ostwald De Waele model	H	total head
η	Pump efficiency = $\rho \cdot Q \cdot g \cdot H / P_{shaft}$	k	consistency index
μ	dynamic viscosity	n	viscosity index
μ_a	apparent dynamic viscosity	N	rotational speed in rpm
μ_0	zero shear viscosity	N_p	Power number
μ_t	eddy viscosity	n_q	specific speed
ν	kinematic viscosity	P_{df}	disc friction losses
ρ	Density	P_{shaft}	shaft power
ω	rotational speed in rad/s	P_v	volute losses
		Q	volume flow rate
		Re_u	Reynolds number

INTRODUCTION

For Newtonian fluid the stress response σ to a simple shear rate $\dot{\gamma}$ is linear (Eq. 1) and the linearity constant μ is exclusively a function of the state of the fluid (density, pressure and temperature).

$$\sigma = \mu \cdot \dot{\gamma} \quad (1)$$

A non-Newtonian fluid is an exception to this behavior so an “apparent viscosity” μ_a must be defined. There are many classes of non-Newtonian fluid so one unique and universal model suitable for all situations does not exist (Steffe, 1996). A well-known formulation for a time-independent non-Newtonian fluid is the Power Law fluid model that is defined in Eq. 2, where: (i) $\dot{\gamma}$ is the shear rate, defined as the velocity gradient perpendicular to the main direction, $\partial u/\partial y$; (ii) the consistency

coefficient k is a constant which depends on the specific fluid; (iii) n is the power law index that defines the pseudoplastic ($n < 1$) or dilatant ($n > 1$) behavior of the fluid (Jacobs, 1996)

$$\mu_a = k \cdot \dot{\gamma}^{n-1} \quad (2)$$

The determination and measurement of the model parameters and the reproducibility of experimental data is critical, because the overall fluid characteristics vary, not only with the fluid, but also with respect to the different conditions in which it is used. Despite the significant advances made in this field, the choice of an appropriate constitutive relation, which depends on the fluid characteristics and the process parameters, is guided by intuition and by experience (Chhabra, 2010).

Special duty rotordynamic (centrifugal) pumps are the most common type of pump used in the chemical industry (Chhabra, 1999) and in hygienic applications (Karassik et al., 2008) because of their simplicity and limited cost, their smooth flow delivery and their easy maintenance. They could also find wide approval in non-Newtonian or high viscosity fluid applications. In these cases, the pump performance in terms of head, flow rate and efficiency can degrade consistently. For centrifugal pumps a fluid viscosity of 300-500 cP is considered the threshold of appreciable efficiency reduction (Karassik et al., 2008, Nesbitt, 2003). Moreover, the modification of the local Reynolds number can impact on the inner flow regime. The distribution of the shear in centrifugal pumps varies the throughput. While the pump is working, the difference of the shear rate within the pump regions (rotor-volute gap, rotor vanes and volute discharge) are less extreme. Another problem that may occur is at the start, because the high apparent viscosity affects the pump performance causing the overloading of the motor (Chhabra, 1999).

Pump design is always carried out by considering water as the working fluid and then by applying empirical correction to performance, according to the actual fluid processed by selecting a suitable value of the apparent viscosity (Chhabra, 1999), so every fluid needs its own empirical study. The correlation diagram for the correction factor to apply in the case of viscous fluids can be found in the Engineering Reference Book of Energy and Heat (1991).

CFD techniques allow the analysis of the impact of the fluid change and the effectiveness of the design correction, providing comprehensive data that are not easily obtainable from experimental tests. The main advantage of CFD over experimental techniques is that, against an experimental validation with conventional fluids (i.e. water), CFD enables the study and the assessment of the performances of different types of pumps working with different types of fluid, without building a specific test rig for a specific fluid. For this reason, CFD techniques are used in the design and optimization of industrial products and in the process industry, such as mixing technology and anaerobic digesters where high viscosity or non-Newtonian fluids are present.

In literature, before of the latest years, there was a lack of knowledge about the behavior of centrifugal pumps handling the following kind of fluids: (i) high viscosity fluids, which are characterized by a viscosity significantly higher than water and (ii) non-Newtonian fluids, whose rheology follows a non-Newtonian law. In J.J.N. Kalombo et al. (2014) two empirical correction approaches for high viscous fluids is tested on two different non-Newtonian slurries. In Shah et al. (2013) a recent review regarding the use of CFD technique applied to centrifugal pump design is presented. Among the non-Newtonian flow applications, they describe the cases of slurry fluid in mining and chemical industry application, and the case of blood pumps. Pagalthivarathi et al. (2011) present an interesting CFD study focused on the flow field within the casing of a centrifugal pump for dense slurries flow. A more developed use of CFD in non-water fluids is in medical applications, especially blood pump applications, where centrifugal pumps are widely used because their capability to produce a smoother flow than axial pumps decreases the probability of blood damage (Behbahani et al., 2009). Burgreen et al. (2001) successfully applied the CFD-based design on a rotary blood pump and compared numerical and experimental results of pump performance and pressure distribution along the length of the pump housing. They validated the numerical simulation performed with a fluid set-up with Newtonian viscosity of 4.0 cP. Li (2000) performed a

comprehensive and detailed experimental analysis of the effects of high viscosity fluids ($48 \text{ mm}^2/\text{s}$) on a centrifugal pump, considering both the pump global performances and the flow pattern within the impeller. He stated that the pump head and power input, in the case of oil, are higher than those for water but the efficiency for oil is lower due to the rapid increase in disc friction losses over the outsides of the impeller hub and shroud as well as the hydraulic losses in the pump flow channel.

Metzner and Otto (1957) studied the mechanical agitation of non-Newtonian fluids with centrifugal impellers which have some similarities with those used in centrifugal pumps. Their work was concerned with the development of a general relationship between impeller speed and the shear rate of the fluid. The resulting relationship was then used to correlate power consumption data on a set of non-Newtonian fluids in a similar way to the Newtonian fluids.

The aim of this work is to study a centrifugal pump for the handling of tomato paste by means of CFD analysis. A sensitivity analysis has been performed in order to assess the correctness of the flow model used for the simulation, i.e. the suitability of using turbulence models with different sensitivity to laminar/turbulent regime, or, when necessary, the suitability of using a laminar model even if the flow in centrifugal pumps can be considered inherently turbulent. As the working fluid, three situations were investigated: (i) standard water, (ii) virtual fluids with increasing dynamic viscosity (up to 6 orders of magnitude higher than water) and (iii) tomato paste, which is a non-Newtonian fluid, with different values of the exponent of the Power Law (viscosity index n) which define its rheological behavior. A simulation campaign was then performed to investigate the pump performances (head, efficiency) with Newtonian high viscosity fluids to investigate the behavior of the pump with respect to the case of the tomato paste working fluid (non-Newtonian high viscosity fluid).

CENTRIFUGAL PUMP FOR TOMATO PASTE APPLICATION

The pump which is the subject of this paper was obtained as a result of a collaboration between an industrial partner and the Engineering Department of the University of Ferrara. The pump was specifically conceived for working with tomato paste. The application is a tomato paste production plant composed of a circuit with three evaporation stages for the extraction of the water from tomato paste. Usually, due to the high viscosity of this fluid, volumetric pumps can be used for their robustness and the almost complete insensitivity to viscosity. However, the ever increasing need for higher productions to follow market requests requires very high volumetric flow rates, so the best choice can be centrifugal pumps with backward blades with a high specific speed, which, conversely, are very sensitive to viscosity.

The original design was carried out using water as the working fluid, with a 1D/2D statistical approach for the inlet and outlet diameters, passage width and blade angles. A potential flow analysis was carried out in order to optimize the meridional passage shape and the blade surface was determined by the conformal representation method. Then, in order to evaluate the performance of the pump with the tomato paste, a correction factor was calculated by correlations in the KSB manual (2005) considering the fluid as Newtonian with high viscosity.

The original design performance specification at BEP for water was: volumetric flow rate $Q = 4,500 \text{ m}^3/\text{h}$, total head $H = 18.8 \text{ m}$ and rotational speed $N = 830 \text{ rpm}$. Actually, the tomato paste production plant equipped with the pump underwent several upgrades in order to raise the rotation speed to 903 rpm and consequently the performance for water, scaled according to the similarity laws, are the following: volume flow rate $Q = 4,896 \text{ m}^3/\text{h}$ and total head $H = 22.3 \text{ m}$. The specific speed of the pump n_q is equal to 102.8. Only experimental data regarding the total head and the volumetric flow rate with water are available, so it is not possible to evaluate experimentally the peak efficiency at BEP.

The working fluid is tomato paste with high consistency, which behaves like a viscoelastic fluid. This fluid can be considered a weak gel, whose properties strongly depend on physical-chemical characteristics due to the tomato variety and processing variables. Valencia et al. (2003) investigated the influence of the sieve pore size and breaking temperature on the viscous flow and non-linear

viscoelastic behavior of tomato paste samples. Particle interactions and particle size both play a role determining tomato consistency and therefore viscosity. In particular, large size particles determine high viscosity (Vercet et al., 2002). Moreover, in the analysis of the rheological behavior of tomato paste, particular attention should be paid to the test method: significant decrease in viscosity was found by Valencia et al. (2003) and Barnes (1999) due to wall-depletion phenomena associated to the rheometer geometry and fluid particle size. As demonstrated by Valencia et al. (2003) the viscous behavior fits well with the Bird-Carreau fluid model in the whole shear range studied where a specific rheology analysis on the working fluid is not available.

The layout and high volume flow rates inside the pump prevent the formation of null and low shear strain rate zones, so the elastic behavior can be neglected. A rheological analysis on the tomato paste produced with this specific plant was performed by the manufacturer. The result showed that the power law (Ostwald De Waele model) was the most representative for the viscous behavior of the fluid under investigation (Eq. 2). The parameters for the Power Law, obtained by the experimental analysis are the following: consistency index, $k = 194.12 \text{ Pa s}$, and $n = 0.326$.



Figure 1 Geometry of the tomato paste centrifugal pump and its computational domain.

Unlike the Bird-Carreau fluid model, in the Power Law the zero shear viscosity μ_0 (Chhabra, 1999) is not present, so it is not suitable for very low shear strain rates. Anyway, as can be seen later, the pump under investigation works for a range of viscosity in which the tomato paste does not show the zero viscosity phenomenon.

GEOMETRY AND COMPUTATIONAL MODEL

In order to have the most representative pump geometry possible, a Reverse Engineering procedure was adopted on the manufactured pump, rather than relying on the mathematical CAD model. The Reverse Engineering of the real components was performed by means of a Romer laser scanner 7320SI and the subsequent parametric CAD representations. At first, a 3D polygonal geometry of the actual geometry was generated by interpolating the point cloud derived from the laser scanner by means of Polyworks V12 software. A 3D model was obtained and exported in the CAD software SolidWorks 2012. This procedure allowed a high-fidelity computational domain of the current pump geometry to be obtained.

The computational domain includes the pump casing and two cylindrical ducts at the suction and at the delivery. The pipe that supplies the pump presents a curved section whose radius and length are customized for every installation. In general, the curved section of the inlet duct is large enough to consider the flow completely developed and not disturbed at the inlet section of the pump.

The grid used in the calculations is a hybrid grid (generated by means of ANSYS Meshing) composed of tetrahedral elements on the core and prismatic elements on walls. The grid was realized with the Delaunay advancing front approach, that consists of surface meshing, extrusion of prism layers on wall surfaces and advancing front tetrahedral meshing for the remaining volume. A mesh sensitivity analysis was performed comparing numerical meshes composed of a number of elements that varies between 4 million and 10 million elements. The final mesh is composed of about 9.7 million volume elements. This mesh ensures that the results are grid-independent and limits the required computational effort as shown in Figure 2.

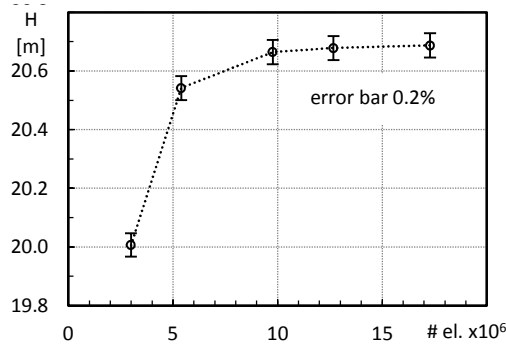


Figure 2 Grid sensibility analysis: the plot shows the value of the total pressure increase with growing number of elements. The grid independence study is performed with water as working fluid and the k- ϵ turbulence model.

CFD ANALYSIS SETUP

The numerical simulations were carried out by means of the commercial CFD code ANSYS CFX 14.5. The code solves the 3D Reynolds averaged form of the Navier–Stokes equations by using an element-based finite volume method. An algebraic multi-grid method based on the additive correction multigrid strategy was used. A second-order high-resolution advection scheme was adopted to calculate the advection terms in the discrete finite volume equations.

The simulations were performed in a steady multiple frame of reference, taking into account the contemporary presence of moving and stationary domains. In particular, a mixing plane approach was imposed at the rotor/stator interface between the impeller and the volute. This type of interface was used for all the simulations. A rotating frame of reference approach was used for the impeller domain with a rotation speed of 903 rpm.

Since pressure and temperature inside the tomato concentration plant are controlled in a limited range, the temperature increments were neglected for the purpose of this study. So, for numerical modeling purposes, the fluids were treated as incompressible and isothermal. Consequently, the energy equation was excluded from the numerical model.

As the inlet boundary condition, a constant velocity value with normal direction and a turbulent intensity equal to 5 % was imposed. The no-slip wall boundary condition was used for all the solid surfaces. For the non-Newtonian fluid the rheological model used is the Ostwald De Waele model (Eq. 2). The Power Law model presents a singularity for null shear viscosity, while for very high shear strain rate values the viscosity tends to zero. So the viscosity had been "bounded" setting a range for the shear strain rate achievable by the fluid in order to ensure a faster convergence and better stability of the numerical simulations. This limitation is related only to the numerical simulation strategy because the final results should never show values of $\dot{\gamma}$ equal to the range boundaries, otherwise the Power Law fluid model is not respected. The upper value of shear strain rate, $\dot{\gamma}_{max}$, and the lower one, $\dot{\gamma}_0$, were chosen equal to 10^7 s^{-1} and 10^{-4} s^{-1} , respectively (Eq. 3). In general, for lower values of shear strain rate the tomato begins to show the zero-viscosity phenomenon, as observed by Sanchez et al. (2003), that is not modeled with the Power Law fluid model.

$$\mu_a = \begin{cases} k \cdot \dot{\gamma}_0^{n-1} & \dot{\gamma} < \dot{\gamma}_0 \\ k \cdot \dot{\gamma}^{n-1} & \dot{\gamma}_0 \leq \dot{\gamma} < \dot{\gamma}_{max} \\ k \cdot \dot{\gamma}_{max}^{n-1} & \dot{\gamma} \geq \dot{\gamma}_{max} \end{cases} \quad (3)$$

A simulation campaign was performed using different high-viscosity Newtonian liquids in order to investigate their behavior compared to tomato paste and water in terms of pump performance (total head and efficiency) and three-dimensional fluid flow. The analysis, on a set of virtual non-

Newtonian fluids with variable viscosity index n (Virtual Fluids with non-Newtonian rheology), was performed searching for a relationship between the behavior of the Newtonian and the non-Newtonian fluids. The set of high-viscosity Newtonian liquids (Virtual Fluids with Newtonian rheology) has the same density and consistency index as tomato paste and an increasing value of viscosity in the interval of (0.015-192) Pa·s. All the fluids used are reported in Table 1.

Turbulence Model sensitivity analysis

Usually, in centrifugal pumps the laminar-turbulent transition occurs when the kinematic viscosity ν reaches the value of about $1.0 \text{ e}^{-4} \text{ m}^2/\text{s}$, but can vary with the type of pump, as stated by Gülich (2010). Since the tomato paste density ρ is equal to $1,100 \text{ kg/m}^3$, the dynamic viscosity transition limits for the Newtonian Virtual Fluid is equal to about $0.110 \text{ Pa}\cdot\text{s}$. This value may be subjected to variation due to the high speed and pump dimensions. On account of this, a turbulence sensitivity analysis was done in the case of Virtual Fluid whose viscosity is up to two orders of magnitude higher than the transition limit, $11 \text{ Pa}\cdot\text{s}$, while for viscosities greater than $11 \text{ Pa}\cdot\text{s}$ the flow is assumed to be laminar and no turbulence model is used.

Table 1 Characteristics of the fluids used for the numerical simulations.

Id.	Description	Rheology	Flow Model	ρ [kg/m ³]	μ [Pa·s]	ν [mm ² /s]	n
<i>H2O</i>	<i>Water</i>	<i>Newtonian</i>	<i>Turbulent k-ε</i>	997	$8.899 \cdot 10^{-4}$	$8.926 \cdot 10^{-4}$	-
<i>TOM0.05</i>	<i>Virtual Fluid</i>	<i>Non-Newt.</i>	<i>Turbulent k-ω</i>	1,100	[Ostwald-De Waele]		0.05
<i>TOM0.1</i>	<i>Virtual Fluid</i>	<i>Non-Newt.</i>	<i>Turbulent k-ω</i>	1,100	[Ostwald-De Waele]		0.1
<i>TOM</i>	<i>Tomato paste</i>	<i>Non-Newt.</i>	<i>Turbulent k-ω</i>	1,100	[Ostwald-De Waele]		0.324
<i>TOM0.5</i>	<i>Virtual Fluid</i>	<i>Non-Newt.</i>	<i>Turbulent k-ω</i>	1,100	[Ostwald-De Waele]		0.5
<i>TOM0.7</i>	<i>Virtual Fluid</i>	<i>Non-Newt.</i>	<i>Turbulent k-ω</i>	1,100	[Ostwald-De Waele]		0.7
<i>TOM0.8</i>	<i>Virtual Fluid</i>	<i>Non-Newt.</i>	<i>Turbulent k-ω</i>	1,100	[Ostwald-De Waele]		0.8
<i>N0.015</i>	<i>Virtual Fluid</i>	<i>Newtonian</i>	<i>Turbulent k-ω</i>	1,100	0.015	0.0136	-
<i>N0.25</i>	<i>Virtual Fluid</i>	<i>Newtonian</i>	<i>Turbulent k-ω</i>	1,100	0.25	0.2272	-
<i>N0.5</i>	<i>Virtual Fluid</i>	<i>Newtonian</i>	<i>Turbulent k-ω</i>	1,100	0.50	0.4545	-
<i>N1</i>	<i>Virtual Fluid</i>	<i>Newtonian</i>	<i>Turbulent k-ω</i>	1,100	1	0.9091	-
<i>N5</i>	<i>Virtual Fluid</i>	<i>Newtonian</i>	<i>Turbulent k-ω</i>	1,100	5	4.546	-
<i>N11</i>	<i>Virtual Fluid</i>	<i>Newtonian</i>	<i>Laminar/ Turbulent k-ω</i>	1,100	11	10.00	-
<i>N20</i>	<i>Virtual Fluid</i>	<i>Newtonian</i>	<i>Laminar</i>	1,100	20	18.18	-
<i>N50</i>	<i>Virtual Fluid</i>	<i>Newtonian</i>	<i>Laminar</i>	1,100	50	45.46	-
<i>N100</i>	<i>Virtual Fluid</i>	<i>Newtonian</i>	<i>Laminar</i>	1,100	100	90.91	-

The turbulence models used for the sensitivity analysis are: i) the standard k-ε, because of its proven reliability in applications where high viscosity or non-Newtonian fluids are present (Sukumar et al., 1996, Yu et al., 2000, Pagalthivarthi et al., 2011, Shah et al., 2013), ii) the k-ω because it works well with low Reynolds number flows and it demonstrated reliability in cases of non-Newtonian turbulent flow as shown by Wu (2010, 2011) and iii) the laminar model (no turbulence). First, a comparison between the turbulence models and the laminar model is carried out for the pump working with the fluid N11, characterized by a dynamic viscosity value of $11 \text{ Pa}\cdot\text{s}$. It is possible to notice from Figure 3b that the k-ω gives the same overall performances as the laminar model, while the standard k-ε shows different results. A more detailed analysis performed by calculating the average eddy viscosity value in the impeller computational domain shows that k-ε overestimates the turbulence giving a mean eddy viscosity of about $40 \text{ Pa}\cdot\text{s}$ (4 times the actual dynamic viscosity), within the impeller computational domain. On the contrary, the standard k-ω produces an eddy viscosity value of about $1 \cdot 10^{-6} \text{ Pa}\cdot\text{s}$.

The same comparison was made for the TOM fluid. Figure 3a illustrates the total pressure increment for the simulation with laminar, standard k- ϵ and standard k- ω . As in the case of Virtual Fluid N11, the k- ϵ turbulence model overestimates the pump head and the mean eddy viscosity, whose value within the impeller computational domain is about 55 Pa·s. On the other hand, the standard k- ω shows a mean eddy viscosity value lower than $1 \cdot 10^{-7}$ Pa·s, and the pump performance curve matches the one calculated with the laminar model. A further comparison was made for the Virtual Fluid N1 with the laminar model and the standard k- ω turbulence model. As can be seen from Figure 3b, there are no differences in the overall pump performances. Moreover, the mean and maximum values of the eddy viscosity μ_t reach values of the same order of magnitude as the viscosity of the fluid. Against these considerations, the standard k- ω is chosen as the reference turbulence model for viscosities lower than 11 Pa·s and for the non-Newtonian fluid model.

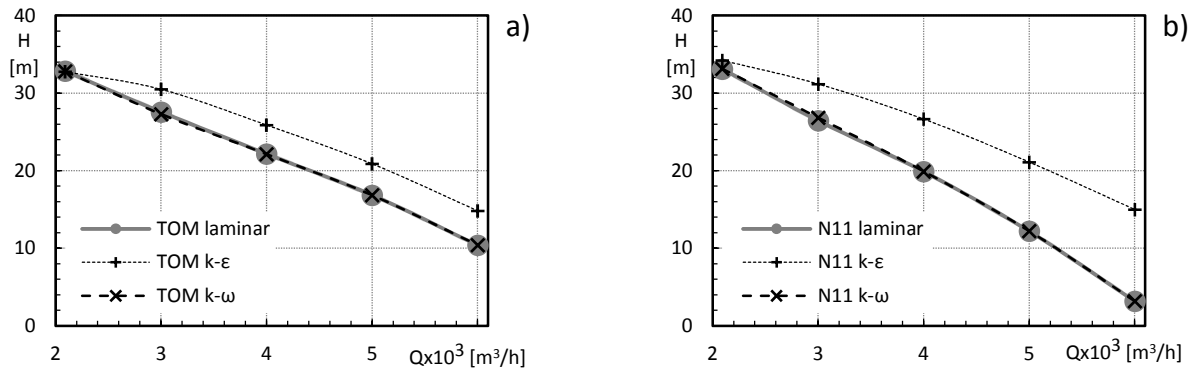


Figure 3 Comparison between the total head for: a) tomato paste (TOM) and b) Virtual Fluid N11; calculated with laminar, k- ϵ and standard k- ω turbulence models.

Numerical model validation

Due to the large dimension of the pump, experimental data either with water or with tomato paste are very difficult to be obtained in dedicated test rigs. So, the only experimental data available can come from the test made by the manufacturer directly on the processing plant. Two manometers (with accuracy of 1.0 % full scale) mounted at the suction and at the delivery of the pump allowed the measurement of the total pressure increment. The volumetric flow rate was measured with a portable clamp-on ultrasound flow sensor, placed in a straight section of the delivery pipe. These clamp-on sensors allow the measurement of flow rates when no sensors are installed and the process cannot be interrupted to insert a flow sensor. However, their accuracy is very low and, in practice, measurement uncertainty values between 6 % to 8 % of the reading should be expected. The rotational speed was measured with a stroboscopic lamp (measurement uncertainty of 0.5 % of the reading), but there are no data about the shaft power. The fluid used for the experimental test was water at ambient temperature. To equip a big size industrial tomato production plant introduced several difficulties: i) the plant was temporarily available so no permanent modification had to be made on the plant, and ii) the plant was big scale (18 meters total height) so the positioning of the instrumentation had to be adapted to the available and feasible measurement sections.

In Figure 4, the comparison between experimental data and numerical results obtained from a simulation of the pump working with water at ambient temperature using the k- ϵ turbulence model is presented. In the Figure, the working points related to the stable part of the performance curve are reported. The error bars on the experimental curve indicate a reference interval of 10 % of measured value to highlight the difference between experimental data and CFD results. The discrepancy of the absolute values can be attributed to the rough experimental setting (in particular, in terms of flow rate sensor accuracy and equipment set up) and the differences in the upstream and downstream geometries of the CFD model compared to the real geometry. In light of this consideration, the authors are confident that the CFD model is representative of the global behavior of the pump.

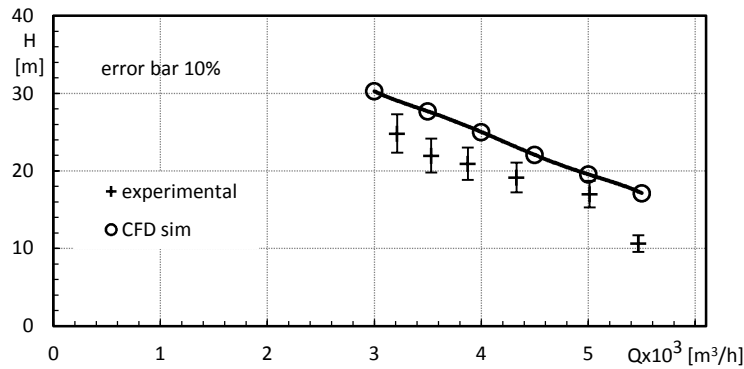


Figure 4 Comparison between experimental data and 3D numerical simulation data (with k- ϵ turbulence model) in terms of total head at 903 rpm with water as the working fluid.

NUMERICAL RESULTS

Overall performances with Newtonian and non-Newtonian fluids

In Figure 5, the performance curves of the high viscosity Virtual Fluids are presented. The trend of the curves is very consistent with empirical data presented in literature, for instance the curves at increasing viscosity reported in Gülich (2010) and the KSB manual (2005). In particular, the viscosity increment leads to the drop in total pressure increment and the BEP moves to a lower volume flow rate. The maximum flow rate and BEP variation is due to the losses (which scale with the viscosity increase) to prevail over the fluid velocity increase made by the impeller. Moreover, the "sudden rising head effect" described in Stepanoff (1993) and Li (2000) cannot be observed because it only appears for small increase of viscosity with respect to water, while the fluids used in this computational analysis have a viscosity much higher than water. For lower flow rates, the head curves tend to the same value of total head, but it cannot be confirmed that they have the same shutoff head as observed by Stepanoff (1993) because this phenomenon depends on the variation of viscosity suffered by the fluid at higher temperatures, which is not the subject of this study. As a final consideration, the fluid TOM shows a behavior similar to the Virtual Fluids N0.5 and N1.

Impeller performances for Newtonian and non-Newtonian fluids

Since the specific speed of the pump is quite high, the disc friction losses are less important in the global energy balance of the machine, as stated by Gülich (2010). In fact, from the numerical results, the disc friction losses are about 5 % of the total shaft power in the cases of the tomato paste and the Virtual Fluid N1, and they increase with the viscosity increase (up to 22 % of the total shaft power for the Virtual Fluid N11). Figures 6a and 6b show that the TOM fluid impeller total head and efficiency curves are always located between the curves of the fluids N0.5 and N1, confirming the similarity between the tomato paste and the Newtonian fluids.

Volute and disc friction losses for Newtonian and non-Newtonian fluids

In Figure 6c it can be observed that for the Newtonian fluids the volute losses has a minimum, this behavior is typical when 3D flow losses prevail over the friction losses. The tomato paste shows instead a clear decrease in losses at lower flow rates which is due to the non-Newtonian rheology. All the fluids has shown a proportionality between the volume mean shear rate and the flow rate, also, since the tomato paste is pseudoplastic, his mean volume apparent viscosity decreased from 36.98 Pa·s at 2,091 m³/h to 16.20 Pa·s at 6,000 m³/h. The lower volute losses at low flow rates for the tomato paste is then attributed to the increase of viscosity that prevent the formation of the 3D flow structures responsible of the losses.

The disc friction losses are the same for every flow rate since they depend on the rotational speed, which is constant. Their magnitude increases with the viscosity for the Virtual Fluids, while the TOM fluid shows values slightly greater than the fluid N1 (Figure 6d).

Impeller flow structures for Newtonian and non-Newtonian fluids

In Figure 7, the comparison of the flow structures at the impeller outlet at 4,000 m³/h for water, TOM, virtual fluid N0.5 and virtual fluid N1 is presented. It can be seen that the viscosity significantly influences the exit flow as reported in Li (2000). The velocity difference between pressure side and suction side is reduced for the high viscosity fluids and there is a clear increase in the boundary layer thickness on the casing side. These results are also observed by Li (2000). The qualitative comparison of the fluid-dynamic structures of the tomato paste with the other fluids shows that the tomato paste has many similarities to the virtual fluids N0.5 and N1.

In Figure 8, a comparison of the impeller tip leakage vortex between water, TOM, virtual fluids N0.5 and N11 is presented. The tip leakage vortex for the TOM fluid and the N0.5 and N11 fluids are greatly reduced with respect to the water. The velocity values again confirm the increase of the boundary layer thickness with increasing viscosity. Once again, the TOM fluid is similar to the virtual fluid N1.

Power consumption-shear rate relationship.

Starting from the Metzner and Otto (1957) work, a relationship between the performances and the shear rate of the pumps was investigated for both the Newtonian and the non-Newtonian fluid sets. Metzner and Otto (1957) assumed that the fluid motion in the region of the impeller was characterized by an average shear rate, linearly related to the speed of the impeller (Metzner, 1957). Since there are similarities between the architecture of centrifugal impellers for the agitation of non-Newtonian fluids and the impeller of the pump, in this paper a similar relationship was investigated. The average shear rate $\bar{\dot{\gamma}}$ was used to calculate the average apparent viscosity $\bar{\mu}_a$;

$$\bar{\mu}_a = k \cdot \bar{\dot{\gamma}}^{n-1} \quad (4)$$

and the machine Reynolds number Re_u for the impeller working with the non-Newtonian fluid.

$$Re_u = \rho \cdot D^2 \cdot \omega / \bar{\mu}_a \quad (5)$$

They observed that the non-Newtonian fluids show a linear Reynolds number-power number relationship, as occurs in the case of the Newtonian fluids; indeed this relationship is only valid for the laminar mixing, not for transition and turbulent mixing.

In this paper, the mean apparent viscosity was evaluated by the volume average on the pump computational domain:

$$\bar{\mu}_a = \frac{1}{V} \int_V \mu_a(\dot{\gamma}) dV \quad (6)$$

Since the purpose of this analysis is to investigate the influence of the fluid type, the working condition used for the numerical comparison is the design point of the impeller pumping water: volumetric flow rate $Q = 4,000 \text{ m}^3/\text{h}$, impeller rotation speed $\omega = 903 \text{ rpm}$.

The power number N_p is defined as follow:

$$N_p = P_{shaft} / (\rho \cdot D^5 \cdot \omega^3) \quad (7)$$

From Figure 9 it can be seen that the linear relationship is confirmed for the Newtonian fluids and is very similar to the one found by Metzner and Otto (1957). The transition from laminar to turbulent behavior for both the Newtonian and non-Newtonian fluid sets can also be seen. For the

non-Newtonian fluids the linear relationship, in the laminar range, is replaced by a Power Law relation between the power number and the Reynolds number calculated.

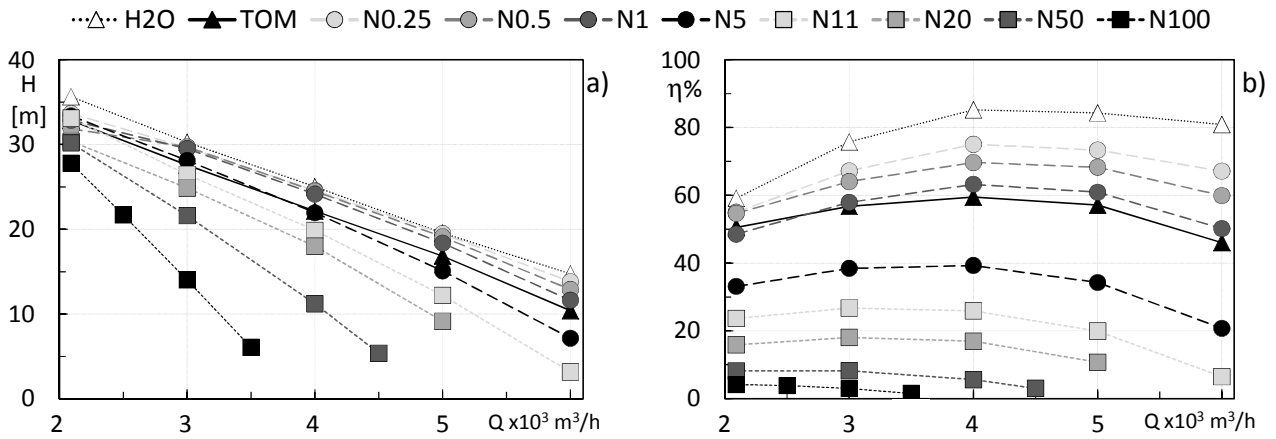


Figure 5 Comparison of the CFD a) pump total head and b) efficiency between the fluids.

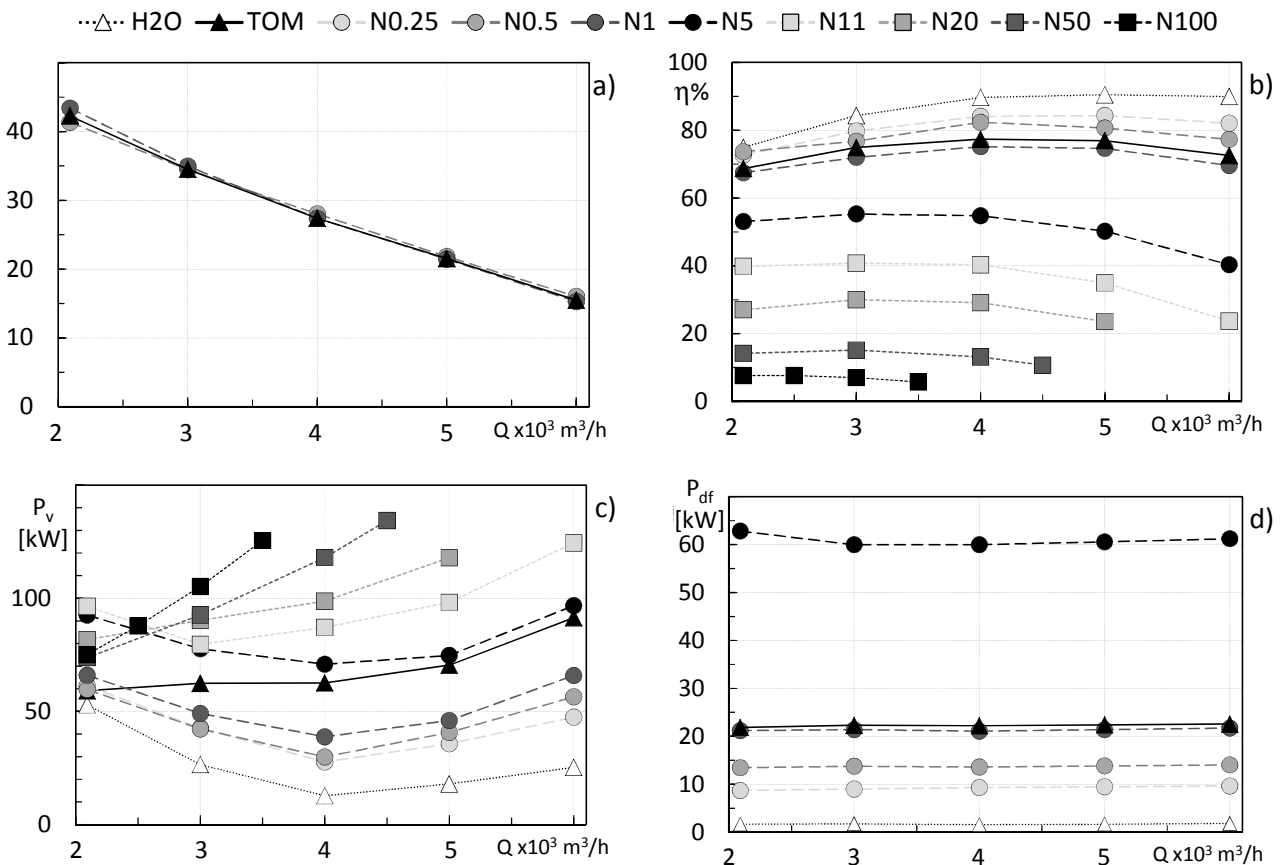


Figure 6 Numerical results comparison: a) impeller total head, b) impeller efficiency, c) volute losses and d) disc friction losses. The impeller total head is total head difference between the trailing edge section and the inlet section of the impeller. The impeller efficiency is calculated using the impeller total head and the shaft power relative to the hub and the blade surfaces.

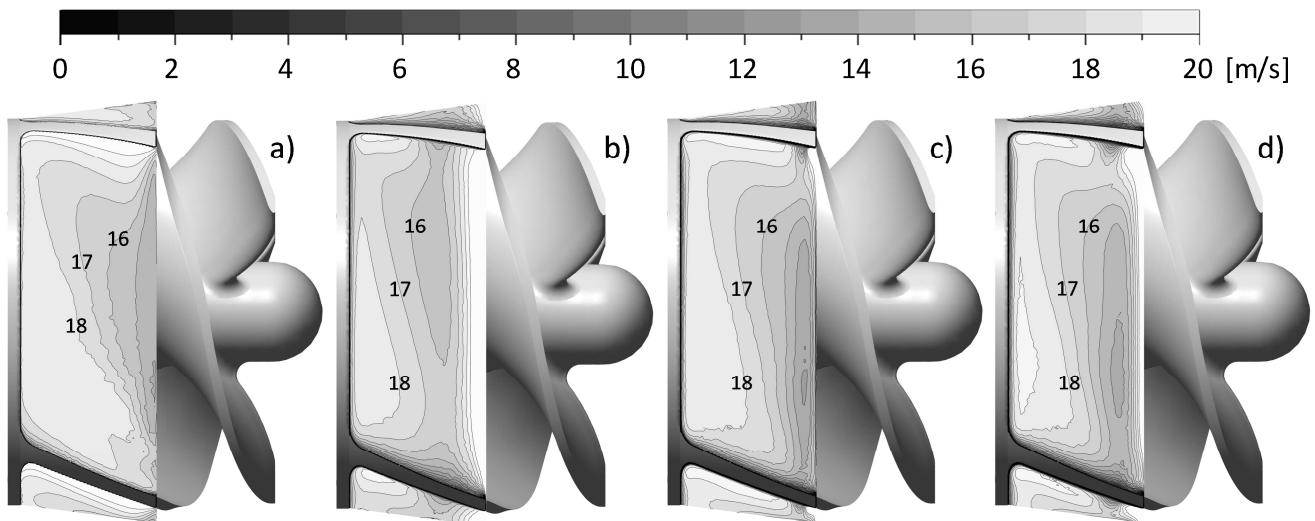


Figure 7 Numerical results comparison of the velocity in the rotating frame of reference at the impeller outlet at 4,000 m³/h: a) water (H₂O), b) tomato paste (TOM), c) Virtual Fluid (N0.5) and d) Virtual Fluid (N1).

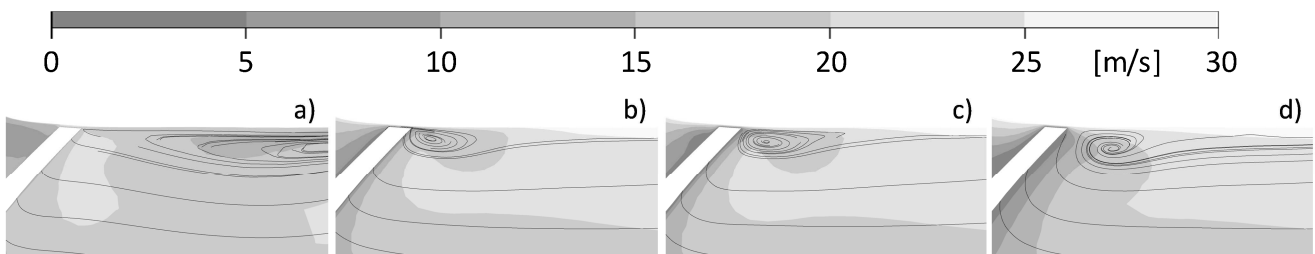


Figure 8 Comparison between the tip leakage flow, at flow rate, $Q = 4,000 \text{ m}^3/\text{h}$ for: a) water (H₂O), b) tomato paste (TOM), c) Virtual Fluid (N1) and d) Virtual Fluid (N11). The contour plots represent the magnitude of relative velocity (velocity in the rotating frame of reference).

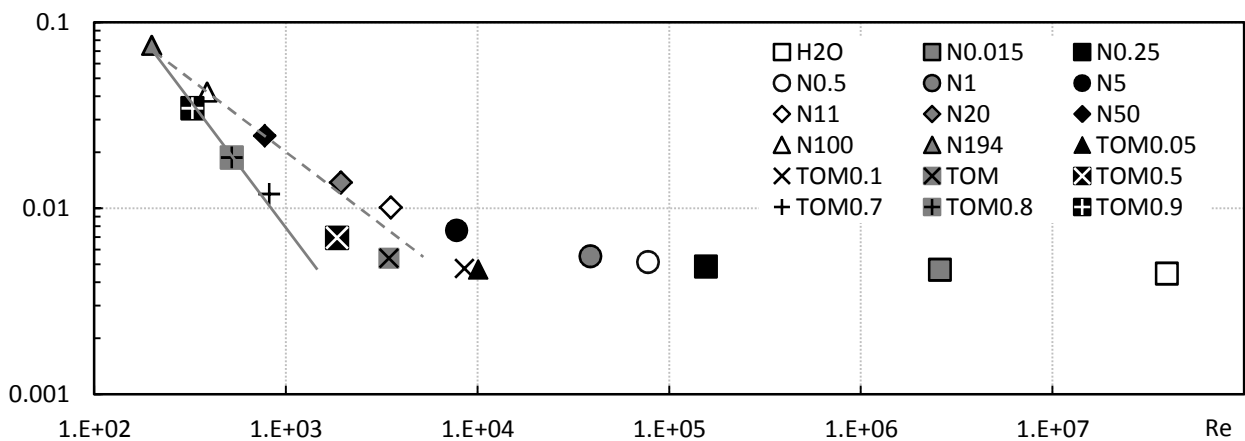


Figure 9 N_p - Re relationship of the Newtonian and non-Newtonian fluid sets.

CONCLUSIONS

A CFD study on a large-size industrial food processing centrifugal pump originally designed for tomato paste has been carried out in order to investigate the similarity and differences between water, tomato paste (non-Newtonian) and high viscosity fluids (Newtonian). To date, pump design has been performed referring to water as the working fluid and then applying correction factors

calculated on the apparent viscosity of the non-Newtonian fluid. Starting from the rheological characterization of the tomato paste, a set of Newtonian fluid with high viscosity has been defined and sensitivity analyses on the flow regime modeling (laminar or turbulent) performed. The CFD study has shown that a fluid viscosity increase affects pump performances coherent with literature data. Then, pump curves and 3D flow structures obtained with non-Newtonian fluid are similar to those obtained with high viscosity Newtonian fluids. In particular, the comparison of the impeller curves of total pressure rise, disc friction losses and efficiency has highlighted a very close trend between tomato paste and Newtonian virtual fluid with a dynamic viscosity value of 1 Pa·s. Great differences have been observed in the volute losses, which has an influence on global pump performances coherent with literature data. A linear relationship between the Reynolds number and the power number of the impeller, for the laminar high viscous Newtonian flow inside the pump was found. A Power Law relationship for a set of virtual non-Newtonian fluids with different viscosity index was also found.

REFERENCES

- ANSYS Inc., CFX User Manual Release 14.5.
- ANSYS Inc., ANSYS Meshing online Help.
- Barnes H.A., (1999), *The yield stress-a review or 'pantarei'-everything flows?*, J. Non-Newtonian Fluid Mech., No.81, 1999, pp.133-178.
- Behbahani M., Behr M, Hormes M., Steinseifer U., Arora D., Coronado O., Pasquali M., (2009), *A Review of Computational Fluid Dynamics Analysis of Blood Pumps*, European Journal of Applied Mathematics, No.20, 2009, pp 363-397.
- Burgreen G.W., Antaki J.F., Wu Z.J., Holmes A.J., (2001), *Computational Fluid Dynamics as a Development Tool for Rotary Blood Pumps*, Artificial Organs, Vol.25, No.5, pp.335-340, Blackwell Science Inc.
- Chhabra R.P., Richardson J.F., (1999), *Non-Newtonian Flow In The Process Industries*, First Edition, Butterworth-Heinemann, Great Britain.
- Chhabra R.P., (2010), *Non-Newtonian Fluids: An Introduction*, SERC School-cum-Symposium on Rheology of Complex Fluids, January 4-9, Indian Institute of Technology Madras, India.
- Engineering Reference Book on Energy and Heat*, (1991), VDI-Verlag GmbH, Düsseldorf.
- Gulich J.F., (2010), *Centrifugal Pumps*, Springer, pp.741-804.
- Jacobs B.E.A., (1991), *Design of Slurry Transport Systems*, Elsevier Science Publisher LTD.
- Kalombo J. J. N., Haldenwang R., Chhabra R. P. and Fester V. G., (2014), *Centrifugal Pump Derating for Non-Newtonian Slurries*, Journal of Fluids Engineering, Vol. 136, Nr. 3, p.031302.
- Karassik I.J., Messina J.P., Cooper P., Heald C.C., (2008), *Pump Handbook*, 4th Edition, The McGraw-Hill Companies Inc., USA.
- KSB Italia S.p.A., (2005), *Selezione delle pompe centrifughe*, New Industrial Foto s.r.l., Italia.
- Li W., (2000), *Effects of viscosity of fluids on centrifugal pump performance and flow pattern in the impeller*, Int. Journal of Heat and Fluid Flow, Vol.21, 2000, pp.207-212.
- Metzner A. B., Otto R. E., (1957), *Agitation of Non-Newtonian Fluids*, AIChE Journal, Vol.3, Nr. 1, 1957, pp.3-10.
- Nesbitt B., (2003), *Pumps for food and drink*, World Pumps, Elsevier Ltd., August 2003, pp.22-27.
- Pagalthivarthi K.V., Gupta P.K., Tyagi V., Ravi M.R., (2011), *CFD Predictions of Dense Slurry Flow in Centrifugal Pump Casings*, World Academy of Science, Engineering and Technology, Vol.5, No.3, 2011, pp. 16-28.
- Sanchez M.C., Valencia C., Ciruelos A., Latorre A., Galleos C., (2003), *Rheological Properties of Tomato Paste: Influence of the Addition of Tomato Slurry*, Journal of Food Science, Vol.68, Nr.2,

2003, pp.551-554. Shah S.R., Jain S.V., Patel R.N., Lakhera V.J., *CFD for centrifugal pumps: a review of the state-of-the-art*, Procedia Engineering, No.51, 2013, pp.715-720.

Steffe J.F., “*Rheological Methods in Food Processing Engineering*”, Second Edition, 1996, Freeman Press.

Stepanoff A.J., (1993), *Centrifugal and Axial Flow Pumps*, 2nd Edition, Krieger Publishing Company, Malabar, Florida.

Sukumar R., Athavale M.M, Makhijani V.B., Przekwas A.J., (1996), *Application of Computational Fluid Dynamics Techniques to Blood Pumps*, Artificial organs, Vol.20, No.6, pp.529-533.

Valencia C., Sanchez M.C., Ciruelos A., Latorre A., Madiedo J.M., Gallegos C., (2003), *Non-linear viscoelasticity modeling of tomato paste products*, Food Research Int. , Vol.36, 2003, pp.911-919.

Vercet A., Sanchez C., Burgos J., Montañes L., Lopez Buesa P., (2002), *The effects of monothermosonication on tomato pectic enzymes and tomato paste rheological properties*, J. of Food Engineering, Vol. 53, 2002, pp.273-278.

Wu B., (2010), *Computational fluid dynamics investigation of turbulence models for non-Newtonian fluid flow in anaerobic digesters*, Environmental Science & technology, Vol.44, 2010, pp.8989-8995.

Wu B., (2011), *CFD investigation of turbulence models for mechanical agitation of non-Newtonian fluids in anaerobic digesters*, Water Research, Vol.45, 2011, pp.2082-2094.

Yu S.C.M., Ng B.T.H., Chan W.K., Chua L.P., (2000), *The flow patterns within the impeller passages of a centrifugal blood pump model*, Medical Engineering & Physics, Vol.22, 2000, pp.381-393.